JBC RESEARCH ARTICLE

Blockade of CD47 function attenuates restenosis by promoting smooth muscle cell efferocytosis and inhibiting their migration and proliferation

Received for publication, December 28, 2022, and in revised form, March 4, 2023 Published, Papers in Press, March 8, 2023,
https://doi.org/10.1016/j.jbc.2023.104594

Suresh Govatati, Prahalathan Pichavaram, Raj Kumar, and Gadiparthi N. Rao*

From the Department of Physiology, University of Tennessee Health Science Center, Memphis, Tennessee, USA

Reviewed by members of the JBC Editorial Board. Edited by George M. Carman

Cluster of differentiation 47 (CD47) plays an important role in the pathophysiology of various diseases including atherosclerosis but its role in neointimal hyperplasia which contributes to restenosis has not been studied. Using molecular approaches in combination with a mouse vascular endothelial denudation model, we studied the role of CD47 in injury-induced neointimal hyperplasia. We determined that thrombin-induced CD47 expression both in human aortic smooth muscle cells (HASMCs) and mouse aortic smooth muscle cells. In exploring the mechanisms, we found that the protease-activated receptor 1-Gα protein q/11 (Gαq/11)–phospholipase Cβ3–nuclear factor of activated T cells c1 signaling axis regulates thrombin-induced CD47 expression in HASMCs. Depletion of CD47 levels using its siRNA or interference of its function by its blocking antibody (bAb) blunted thrombin-induced migration and proliferation of HASMCs and mouse aortic smooth muscle cells. In addition, we found that thrombin-induced HASMC migration requires CD47 interaction with integrin β3. On the other hand, thrombin-induced HASMC proliferation was dependent on CD47's role in nuclear export and degradation of cyclin-dependent kinase–interacting protein 1. In addition, suppression of CD47 function by its bAb rescued HASMC efferocytosis from inhibition by thrombin. We also found that vascular injury induces CD47 expression in intimal SMCs and that inhibition of CD47 function by its bAb, while alleviating injury-induced inhibition of SMC efferocytosis, attenuated SMC migration, and proliferation resulting in reduced neointima formation. Thus, these findings reveal a pathological role for CD47 in neointimal hyperplasia.

Vascular smooth muscle cell (VSMC) migration and proliferation play a crucial role in the development of neointimal hyperplasia following percutaneous transluminal angioplasty (1). Cluster of differentiation 47 (CD47) also known as integrin associated protein is a ubiquitously expressed transmembrane glycoprotein that has been implicated in many normal and pathophysiological processes, including apoptosis, cell adhesion, cell migration & proliferation, and inflammation (2–6). In recent years, it was demonstrated that CD47, as a bona fide "don't eat me" molecule, inhibits efferocytosis and thereby leads to the accumulation of cell debris in aortic plaques and as a result in the progression of atherosclerosis (7–11). Although the role of CD47 in vascular diseases, particularly in atherosclerosis and stroke, has been studied (12, 13), very little is known on its role in neointimal hyperplasia. Previously, it was reported that activation of CD47 elicits proliferative response in cultured smooth muscle cells (SMCs) and that mechanical vascular injury increases its expression in the medial and neointimal region (14). In addition, CD47 has been shown to inhibit inflammatory response triggered by the placement of stents and suppress in-stent restenosis (15, 16). Neointimal hyperplasia that occurs after vascular interventions such as angioplasty, stent implantation, endarterectomy, and bypass grafting is a major contributing factor in restenosis and in-stent restenosis (17). Phenotypic switching of SMCs from contractile to synthetic state and their subsequent migration from media to tunica intima leading to their enhanced proliferation in the intima is the primary cause of neointimal hyperplasia (18, 19). Thus, exploring mechanisms underlying SMC migration and proliferation may lead to the development of new therapeutic targets against restenosis and in-stent restenosis. In response to injury, SMCs secrete an array of molecules that play a key role in vascular wall remodeling (20). In addition, vascular injury induces the generation of thrombin, a potent mitogen, and chemotactic factor, in a time-dependent manner (21). The recent work from our laboratory showed that thrombin *via* inducing the expression of interleukin-33 (IL-33) and cell division cycle 6 (CDC6) mediates VSMC migration and proliferation, respectively, leading to injury-induced vascular wall remodeling (22–24). Since vascular injury induces CD47 expression and its role in SMC proliferation and in-stent restenosis has been reported previously (14–16), we asked whether CD47 plays a role in thrombin-induced SMC migration and proliferation and injury-induced neointimal hyperplasia. In the present study, we show that CD47 while inhibiting SMC efferocytosis also mediates SMC migration and proliferation *in vitro* in response to thrombin and *in vivo* in response to injury, leading to neointimal hyperplasia and vascular wall remodeling.

* For correspondence: Gadiparthi N. Rao, rgadipar@uthsc.edu.

Results

CD47 mediates thrombin-induced VSMC migration and proliferation

Previous studies have reported increased expression of CD47 in injured arteries as well as atherosclerotic plaques (7, 14). We have shown that thrombin– protease-activated receptor 1 (PAR1) signaling plays a role both in neointimal hyperplasia and atherosclerosis (22–25). Based on these clues, we asked whether CD47 has any role in thrombin-induced vascular wall remodeling. To test this, first, we studied a time course effect of thrombin on CD47 expression in human aortic smooth muscle cells (HASMCs). We found that thrombin (0.5 U/ml) induces CD47 expression both at mRNA and protein levels in HASMCs in a time-dependent manner (Fig. 1, *A* and *B*). Immunofluorescence staining also showed a robust induction of CD47 in thrombin-treated HASMCs (Fig. 1*C*). Based on these observations, we next examined for the functional significance of CD47 in HASMCs. Depletion of CD47 levels by its siRNA (siCD47) substantially attenuated thrombin-induced HASMC migration and proliferation (Fig. 1, *D* and *F*). Cell viability by Trypan blue exclusion assay showed <5% of cell death both in siControl and siCD47-transfected cells. These results clearly infer that the decrease in thrombin-induced HASMC migration and proliferation by siCD47 was due to its effect on CD47 depletion rather than its cytotoxicity. Furthermore, interference with CD47 function by its blocking antibody (bAb, B6.H12; 10 μg/ml) also blunted thrombin-induced HASMC migration and proliferation (Fig. 1, *E* and *G*). Since our recent findings showed species-specific posttranslational modification of LMCD1 (LIM and cysteine-rich domains protein 1), a key transcriptional coregulator, in the modulation of VSMC migration and proliferation (24), we then tested for CD47 species specificity in thrombin-induced VSMC migration and proliferation. First, consistent with its expression in HASMCs, CD47 was also induced in mouse aortic smooth muscle cells (MASMCs) in response to thrombin (Fig. 1, *H* and *I*). Second, interference with CD47 function by its bAb (MIAP301; 10 μg/ml) attenuated thrombin-induced MASMC migration and proliferation as well (Fig. 1, *J* and *K*). Together, these results indicate that CD47 plays an important role in thrombin-induced VSMC migration and proliferation both in humans and mice.

PAR1-Gαq/11-PLCβ3-NFATc1 signaling is required for thrombin-induced CD47 expression

Previously, we have reported that activation of nuclear factor of activated T cells c1 (NFATc1), E2F1 (E2F transcription factor 1), and LMCD1 downstream to PAR1-Gαq/11 (Gα protein q/11)-phospholipase Cβ3 (PLCβ3) signaling was required for thrombin-induced IL-33 and CDC6 expression-mediating HASMC migration and proliferation, respectively (22–24). In view of these observations, we next studied the role of this signaling in thrombin-induced CD47 expression. Downregulation of PAR1, Gαq/11, PLCβ3 or NFATc1 but not E2F1 or LMCD1 levels using their respective siRNAs attenuated thrombin-induced CD47 expression both at mRNA and protein levels in HASMCs (Fig. 2, *A*–*H*). Previous studies have reported that endothelin-1 also stimulates NFATc1 *via* Gαq/11-PLCβ signaling in cardiac myocytes and neuronal crest cells (26, 27). Therefore, to demonstrate PAR1 specificity on NFATc1 activation, we examined for its involvement in endothelin-1-induced NFATc1 activation. Blockade of PAR1 by its antagonist SCH79797 (10 μM) while negating thrombin-induced NFATc1 activation, as measured by its nuclear translocation, had no effect on endothelin-1-induced NFATc1 activation in HASMCs (Fig. 2*I*). These observations clearly show the specificity of PAR1-Gαq/11-PLCβ3 signaling in thrombin-induced NFATc1 activation and its role in CD47 expression.

Interaction of CD47 with integrin β3 is required for thrombin-induced HASMC migration

CD47 is a multifunctional glycoprotein and exerts its biological effects by binding with various cell-surface receptors as well as extracellular matrix proteins (28). Thrombospondin 1 (TSP1), signal regulatory protein α (SIRPα), and integrins, particularly integrin αVβ3, are the high-affinity signaling partners of CD47 in mediating its biological effects in response to various cues (28–33). Therefore, to understand the mechanisms by which CD47 mediates HASMC migration and proliferation, first, we studied a time course effect of thrombin on the expression of these molecules in HASMCs. We found that thrombin (0.5 U/ml) while having no effect on integrin αVβ3 levels, downregulated the expression levels of both TSP1 and SIRPα in HASMCs (Fig. 3*A*). Next, we tested the interaction of CD47 with TSP1, SIRPα, and integrin αVβ3 in response to thrombin. CD47 interacts only with integrin β3 but not TSP1, SIRPα, or integrin αV in response to thrombin (Fig. 3*B*). In addition, integrin β3 that was complexed with CD47 was found to be highly phosphorylated at Y773 and Y785 residues (Fig. 3*B*). A role for integrin β3 tyrosine phosphorylation in VSMC migration and proliferation in response to various agonists has been reported previously (34–37). To confirm the interactions between CD47 and integrin β3, we also performed coimmunofluorescence staining and proximity ligation assay (PLA). Our findings showed that CD47 interacts with integrin β3 in response to thrombin as demonstrated by coimmunofluorescence staining as well as PLA (Fig. 3, *C* and *D*). To explore the functional significance of these interactions, we next studied the role of these molecules in thrombin-induced HASMC migration and proliferation. In line with the lack of the effect of thrombin on CD47 interaction with TSP1 or SIRPα, blockade of their function by their neutralizing antibodies had no effect on thrombin-induced HASMC migration and proliferation (Fig. 3, *E*–*G*). However, consistent with enhanced interaction of integrin β3 with CD47 in response to thrombin, interference with integrin β3 function by its neutralizing antibody while having minimal effect on proliferation blocked thrombin-induced HASMC migration (Fig. 3, *E* and *H*). These findings imply that integrin β3 but not TSP1 or SIRPα is required for thrombin-induced CD47-mediated HASMCs migration.

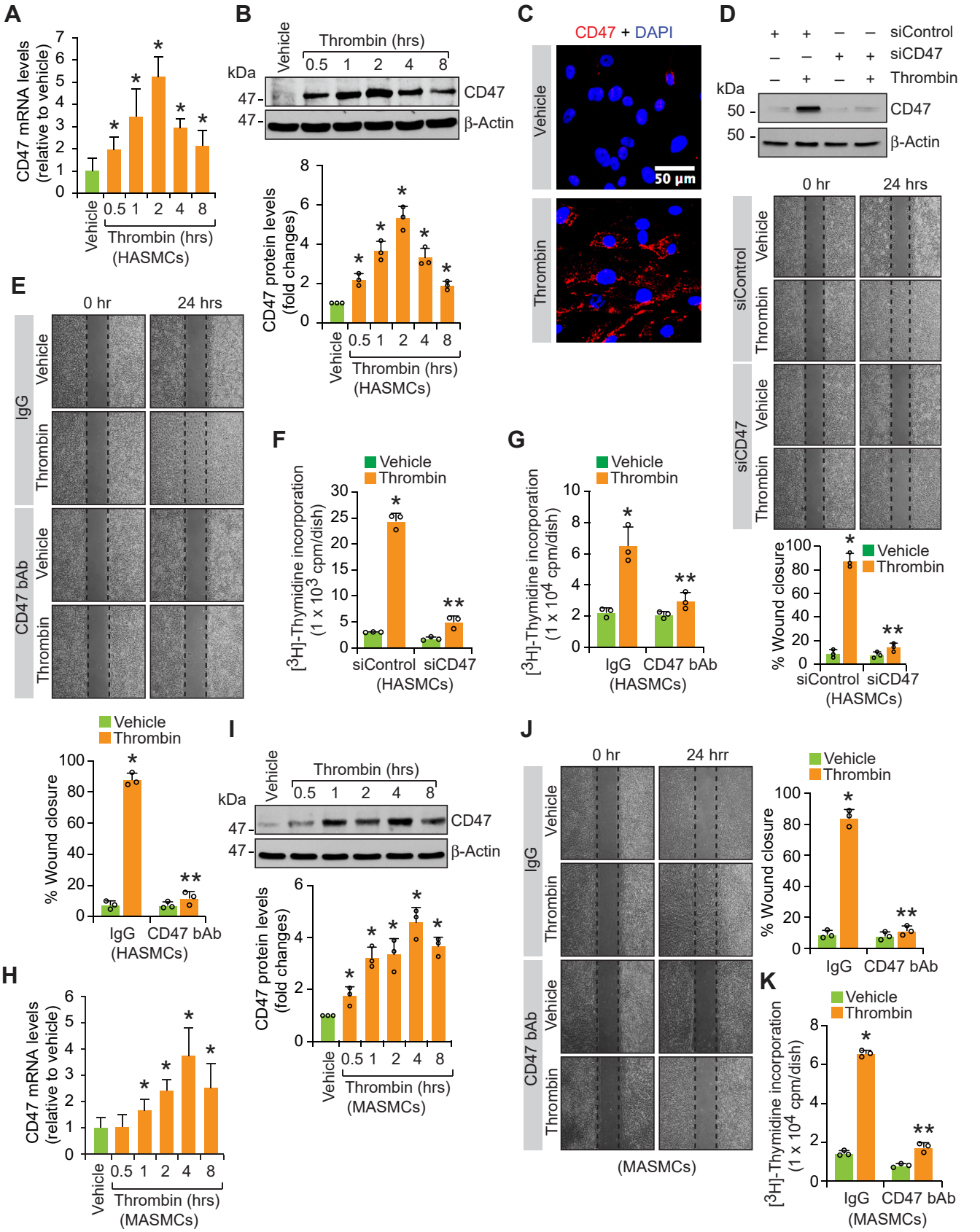

Figure 1. CD47 mediates thrombin-induced VSMC migration and proliferation. *A*, *B*, *H*, and *I*, quiescent HASMCs (*A* and *B*) or MASMCs (*H* and *I*) were treated with and without thrombin (0.5 U/ml) for the indicated time periods, either RNA was isolated and analyzed by qRT-PCR for CD47 and β-actin mRNA levels using their specific primers (*A* and *H*) or cell extracts were prepared and analyzed by Western blotting for CD47 and β-actin levels using their specific antibodies (*B* and *I*). The n is three for panels *A*, *B*, *H*, and *I*. *C*, quiescent HASMCs were treated with and without thrombin (0.5 U/ml) for 2 h, fixed, and

CD47 is required for thrombin-induced p21Cip1 nuclear export and its degradation in mediating HASMC proliferation

Since activation of integrin β3 is required only for thrombin-induced HASMC migration but not proliferation, we wanted to explore the mechanisms by which CD47 mediates thrombin-induced HASMC proliferation. We have previously reported that p21 cyclin-dependent kinase–interacting protein 1 (p21Cip1) translocated from the nucleus to the cytoplasm and undergoes proteasomal-mediated degradation in the modulation of monocyte chemoattractant protein 1-induced HASMC proliferation (38). Based on this information, we asked whether thrombin induced CD47-mediated HASMC proliferation requires p21Cip1 nuclear export and its degradation. To address this, first, we studied the effect of thrombin on CDK inhibitors in HASMCs. While having no major effect on the steady state levels of p27Kip1 or p57Kip2, thrombin downregulated p21Cip1 levels in a time-dependent manner (Fig. 4*A*). Thrombin had no apparent effect on p21Cip1 mRNA levels as compared to vehicle control (Fig. 4*B*). To understand the mechanism by which thrombin downregulates p21Cip1, we next examined its nuclear export, as mitogens trigger its translocation from the nucleus to the cytoplasm, where it undergoes degradation (39, 40). First, in control cells, most of p21Cip1 remained in the nucleus; however, in response to thrombin its levels both in the nucleus and cytoplasm appear to be decreased (Fig. 4, *C*–*F*). In addition, depletion of CD47 levels or blockade of its function led to the accumulation of p21Cip1 in the nucleus in response to thrombin, suggesting its role in p21Cip1 nuclear export (Fig. 4, *C*–*F*). To gain more evidence supporting this observation, we tested for CD47 and p21Cip1 interactions in the presence and absence of MG132, a proteasomal inhibitor (41). In response to thrombin, CD47 was found to be associated with p21Cip1 only in the cytoplasm but not in the nucleus and that in the presence of MG132 their interactions were further stabilized (Fig. 4*G*). In addition, coimmunofluorescence staining revealed the interaction of CD47 with p21Cip1 only in the cytoplasm in response to thrombin (Fig. 4*H*). Moreover, in the presence of MG132, p21Cip1 was stabilized and as such its association with CD47 particularly in the cytoplasm in response to thrombin was also increased (Fig. 4*H*). These observations reveal that CD47 while facilitating p21Cip1 nuclear export also binds with p21Cip1 in the cytoplasm and leads to its proteasomal-mediated degradation. In view of these observations, we next studied the effect of MG132 on thrombin-induced HASMC proliferation. MG132 substantially blocked thrombin-induced HASMC proliferation (Fig. 4*I*). Together, these observations reveal that CD47 binds with and mediates proteasomal degradation of p21Cip1 in the cytoplasm in response to thrombin in the modulation of HASMC proliferation.

CD47 mediates neointimal hyperplasia via modulation of VSMC migration and proliferation

To understand the role of CD47 in injury-induced neointima formation *in vivo*, we used a mouse femoral artery guidewire injury (GI) model. In line with the effect of thrombin on CD47 expression in HASMCs and MASMCs *in vitro*, GI also induced CD47 expression in mouse femoral arteries in a time-dependent manner with maximum effect at 7 days post GI (Fig. 5*A*). In addition, double immunofluorescence staining for CD47 and smooth muscle myosin heavy chain (SMMHC) showed the expression of CD47 mostly in intimal SMCs in response to GI (Fig. 5*B*). Since thrombin-induced CD47 expression requires NFATc1 in HASMCs *in vitro* (Fig. 2*F*), we also wanted to test its potential role in injury-induced CD47 induction. To this end, application of NFATc1 siRNA in Pluronic gel perivascularly *in vivo* depleted GI-induced NFATc1 as well as CD47 expression levels (Fig. 5*C*). This observation suggests a role for NFATc1 in injury-induced CD47 expression. Since SMC migration and invasion from media to intima toward the injured luminal surface and their proliferation in the intimal region are critical factors for the development of neointimal hyperplasia (17), we next tested the role of CD47 in these responses. Interference with CD47 function by its bAb (MIAP301) attenuated GI-induced SMC migration from media to luminal surface and their proliferation (Fig. 5, *D* and *E*). In line with these observations, CD47 bAb (MIAP301) also blunted GI-induced neointima formation substantially (Fig. 5*F*). These results infer that injury triggers CD47 expression in SMCs, which in turn mediates their migration and proliferation leading to neointima formation.

CD47 inhibits SMC efferocytosis

Earlier studies have reported that besides migration and proliferation, apoptosis of SMCs also plays a role in neointimal hyperplasia (42). In recent years, it was further demonstrated that defective efferocytosis (clearance of apoptotic cells) of SMCs as a potential contributing factor in the development of neointimal hyperplasia and atherosclerosis (7, 8). CD47 is a bona fide "don't eat me" molecule and plays an important role in the inhibition of apoptotic cell clearance (2–8). Previous studies have reported that thrombin induces apoptosis of SMCs (43). In view of these observations, we asked whether CD47 has any role in thrombin-induced apoptosis and efferocytosis of SMCs. To this end,

immunostained for CD47 using its specific antibody. The n is three for panel *C*. *D*–*G*, HASMCs that were transfected with siControl or siCD47 (100 nmoles) or preincubated (30 min) with IgG isotype control or CD47 bAb (10 μg/ml) were quiesced and tested for thrombin (0.5 U/ml)-induced migration (*D* and *E*) and proliferation (*F* and *G*). *Top panel* in panel *D* shows the efficacy of siCD47 on the depletion of CD47 levels. The n is three for panels *D*–*G*. *J* and *K*, quiescent MASMCs that were preincubated (30 min) with IgG isotype control or CD47 bAb (10 μg/ml) were tested for thrombin (0.5 U/ml)-induced migration (*J*) and proliferation (*K*). The n is three for panels *J* and *K*. The bar graphs represent the Mean ± SD values of three independent experiments. *$p < 0.01$ *versus* vehicle or siControl + vehicle or IgG + vehicle; **$p < 0.01$ *versus* siControl + Thrombin or IgG + Thrombin. The scale bar in panel *C* represents 50 μm. The scale for panels *D*, *E*, and *J* is 1000 μm from the extreme left to the extreme right for each image. bAb, blocking antibody; CD47, cluster of differentiation 47; HASMC, human aortic smooth muscle cell; MASMC, mouse aortic smooth muscle cell; VSMC, vascular smooth muscle cell.

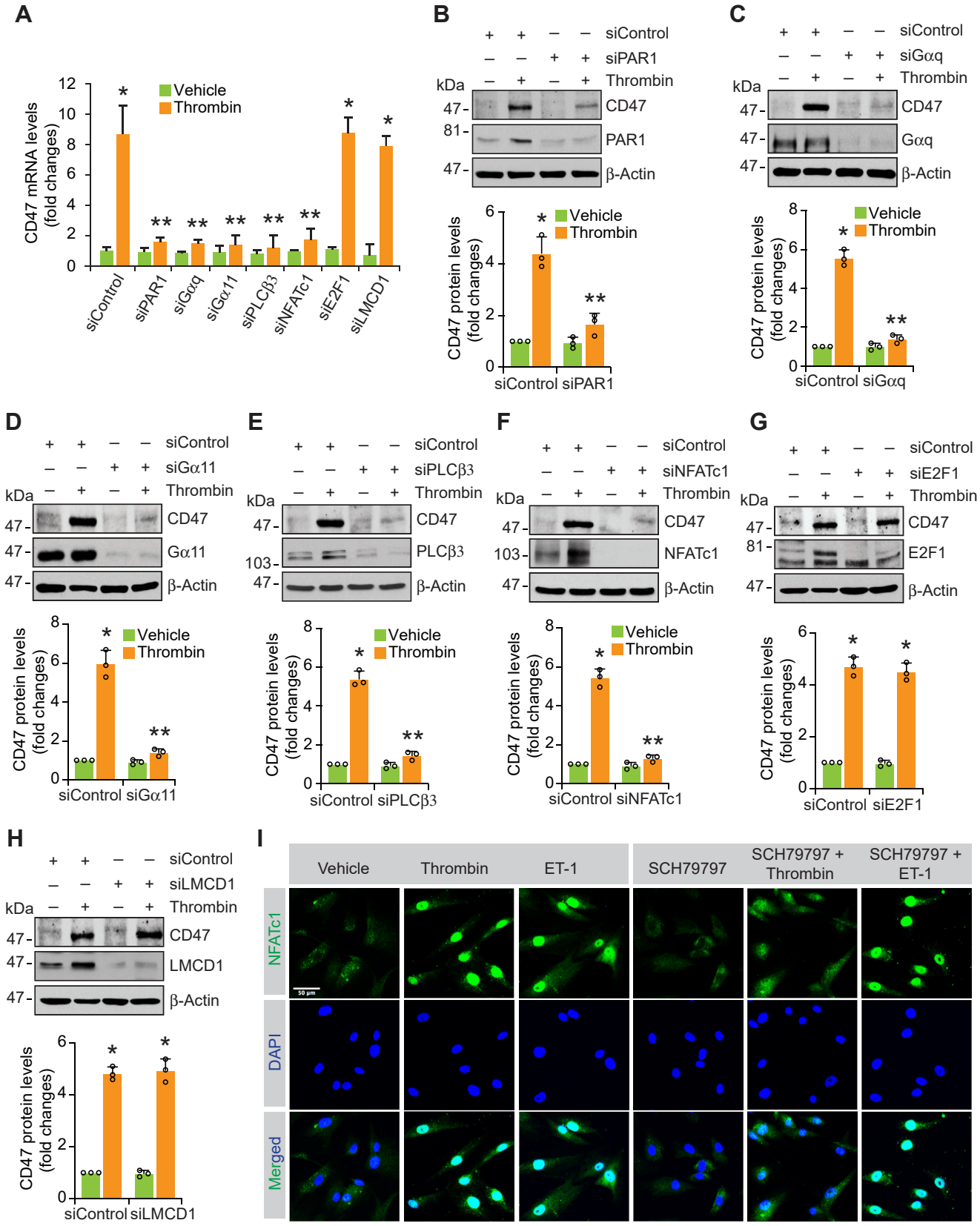

Figure 2. PAR1-mediated Gαq/11-PLCβ3-NFATc1 activation is required for thrombin-induced CD47 expression. *A*, HASMCs were transfected with the indicated siRNA (100 nmoles), quiesced, treated with and without thrombin (0.5 U/ml) for 2 h, RNA was isolated and analyzed by qRT-PCR for CD47 and β-actin mRNA levels using their specific primers. The n is three for panel *A*. *B–H*, all the conditions were the same as in panel *A* except that cell extracts were prepared and analyzed by Western blotting for CD47 and the blots were reprobed for the indicated proteins using their specific antibodies to show the efficacy of the siRNA on its target and off target molecules and/or normalization. The n is three for panels *B–H*. *I*, quiescent HASMCs were treated with and without thrombin (0.5 U/ml) or endothelin-1 (10 nM) in the presence or absence of SCH79797 (10 μM) for 2 h, fixed, and immunostained for NFATc1 using

first, we tested thrombin's effect on HASMC apoptosis and efferocytosis by using *in vitro* apoptosis and efferocytosis assays. Thrombin induced HASMC apoptosis and inhibited basal and staurosporine (STS)-induced HASMC efferocytosis (Fig. 6, *A* and *B*). In addition, inhibition of CD47 function by its bAb while having no effect on thrombin or STS-induced apoptosis reversed HASMC efferocytosis from inhibition by thrombin (Fig. 6, *A*–*C*). Furthermore, siRNA-mediated downregulation of NFATc1 levels restored HASMC efferocytosis from inhibition by thrombin (Fig. 6*D*). Together, these observations suggest that NFATc1-CD47 axis also plays a role in the inhibition of SMC efferocytosis by thrombin. Based on these observations, we next tested the role of efferocytosis in injury-induced neointima formation. Femoral arteries from mice treated with IgG isotype control or CD47 bAb were collected 3 weeks post GI, cross-sections made and stained for SMMHC along with cleaved caspase 3 or CD68, the markers for apoptosis and macrophages, respectively. We observed a few apoptotic SMCs in the neointimal regions of arteries from mice treated with CD47 bAb as compared to mice received IgG isotype control (Fig. 6*E*). In contrast, we found increased number of macrophages (indicative of inflammation) and apoptotic SMCs associated with macrophages (indicative of active efferocytosis) in the neointimal regions of arteries from mice received CD47 bAb as compared to mice received IgG isotype control (Fig. 6*F*). These findings infer that CD47, *via* inhibition of efferocytosis, promotes accumulation of apoptotic SMCs in injured arteries and thus aids in neointima formation.

Lack of a role for CD47 in SMC dedifferentiation

Dedifferentiation of SMCs plays an important role in vascular wall remodeling in response to injury (17–19). Specifically, in response to injury SMC exhibit decreased levels of contractile proteins such as SMMHC, smooth muscle 22α (SM22α), and αsmooth muscle actin (αSMA) (44–47). In addition, in response to injury thrombin production occurs acutely and plays a role in SMC dedifferentiation (48). In this regard, we wanted to test whether CD47 has any role in thrombin-induced SMC phenotypic switching. In line with earlier findings, thrombin (0.5 U/ml) induced downregulation of SMMHC, SM22α, and αSMA expression both at mRNA and protein levels in HASMCs in a time-dependent manner (Fig. 7, *A* and *B*). However, siRNA-mediated depletion of CD47 had no effect on thrombin-induced downregulation of SMMHC, SM22α, or αSMA expression in HASMCs (Fig. 7*C*). Furthermore, GI also downregulated SMMHC expression levels in mouse femoral arteries and that CD47 bAb had no effect on these levels (Fig. 7*D*). These results indicate that although both thrombin and GI induce SMC phenotypic switching from contractile state to synthetic state, CD47 had no effect on SMC dedifferentiation.

Discussion

CD47, a crucial regulator of "don't eat me signal", *via* inhibition of efferocytosis plays an important role in the pathophysiology of various diseases (2–6). Many recent studies have reported that *via* inhibition of efferocytosis CD47 plays a role in atherosclerosis (7–11). In contrast, one study showed that while CD47 global KO protects against atherosclerosis, its myeloid-specific deletion enhances the development of this vascular lesion (49). These observations indicate that CD47 in cell types other than myeloid cells such as SMCs might be involved in atherosclerosis. Regardless of its cell-specific function in atherosclerosis, its role in neointimal hyperplasia is unclear. Although, both vascular injury and inflammatory stimuli can switch VSMC phenotype from quiescent contractile state to synthetic migratory and proliferative state in influencing neointimal hyperplasia (17–19), the role of efferocytosis in this vascular wall remodeling was debatable due to the presence of a few inflammatory cells in neointimal region. However, irrespective of its role in inhibition of efferocytosis, CD47 has been shown to be involved in the suppression of instent restenosis *via* attenuating inflammatory responses (15, 16). Besides these observations, other studies have shown that CD47 mediates VSMC proliferation *in vitro* and vascular injury induces its expression *in vivo* (14). Based on these findings, we asked whether CD47 plays a role in injury-induced neointimal hyperplasia. To this end, our observations reveal that thrombin, a potent VSMC mitogen and chemotactic factor (21), induces CD47 expression both in human and mouse VSMCs and that siRNA-mediated depletion of CD47 or interference of its function by its bAb inhibits thrombin-induced SMC migration and proliferation. In understanding the mechanisms by which CD47 modulates VSMC migration and proliferation, we found that it interacts with integrin β3. In addition, blockade of integrin β3 function by its nAb attenuated thrombin-induced VSMC migration. A large body of data also showed that integrins particularly integrin β3 plays a role in VSMC migration (34–37). Previous studies have also reported that tyrosine phosphorylation of integrin β3 was required for its role in VSMC migration (35, 36). Since thrombin induced tyrosine phosphorylation of integrin β3, it is likely that integrin β3 *via* its tyrosine phosphorylation interacts with CD47 in mediating VSMC migration. p21Cip1 is a CDK inhibitor and its nuclear export leading to its depletion in the cytoplasm is required for cell cycle progression (50, 51). In exploring the mechanisms by which CD47 mediates VSMC proliferation, we found that CD47 interacts with p21Cip1 in the cytoplasm and facilitates its degradation. This finding was further supported by the observations that depletion of CD47 by its siRNA or interference with its function by its bAb attenuated thrombin-induced nuclear export of p21Cip1 and its degradation in the cytoplasm. Since inhibition of proteasomal activity led to p21Cip1 accumulation in the cytoplasm and CD47 binds only with

its specific antibody. The n is three for panel *I*. The bar graphs represent the Mean ± SD values of three independent experiments. *$p < 0.01$ *versus* vehicle or siControl + vehicle; **$p < 0.01$ *versus* siControl + Thrombin. The scale bar in panel *I* represents 50 μm. CD47, cluster of differentiation 47; HASMC, human aortic smooth muscle cell; PAR1, protease-activated receptor 1; PLCβ3, phospholipase Cβ3; NFATc1, nuclear factor of activated T cells c1.

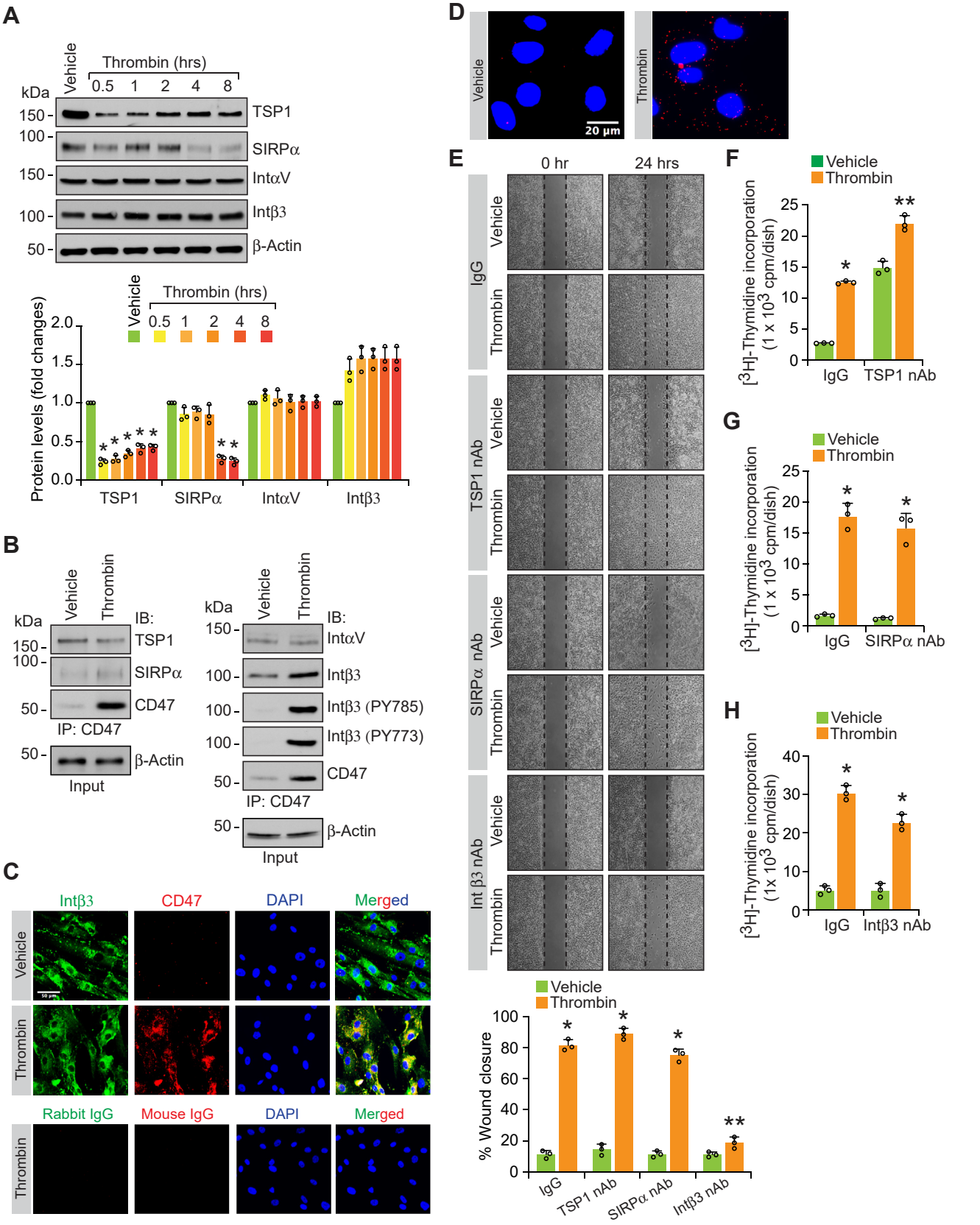

Figure 3. CD47 mediates thrombin-induced HASMC migration *via* interaction with integrin β3. *A*, quiescent HASMCs were treated with and without thrombin (0.5 U/ml) for the indicated time periods, cell extracts were prepared, and analyzed by Western blotting for the indicated proteins using their specific antibodies. The n is three for panel *A*. *B*, quiescent HASMCs were treated with and without thrombin (0.5 U/ml) for 2 h, cell extracts were prepared, immunoprecipitated with the indicated antibodies and the immunocomplexes were analyzed by Western blotting for the indicated proteins using their specific antibodies. The input protein from these samples was analyzed for β-actin levels. The n is three for panel *B*. *C* and *D*, all the conditions were the

cytoplasmic but not nuclear p21Cip1, it appears that CD47 may facilitate p21Cip1 nuclear export and retain it in the cytoplasm for its subsequent ubiquitination and proteasomal-mediated degradation. In line with the *in vitro* observations, CD47 was induced in response to injury and blockade of its function attenuated SMC migration and proliferation resulting in a reduction in injury-induced neointimal hyperplasia. However, further studies are required to explore how a cell surface protein such as CD47 interacts with and promotes p21Cip1 in the cytoplasm.

Although SMC migration and proliferation are the major contributing factors in the development of neointimal hyperplasia, VSMC apoptosis has also been shown to play a role in vascular wall remodeling (42, 52, 53). It was suggested that a subset of apoptotic medial SMCs become resistant to efferocytosis during the acute phase following vascular injury and that in turn trigger a different subset of SMCs to migrate and proliferate to form neointima (54–57). Thus, VSMC apoptosis and their defective efferocytosis could influence neointimal development at least during the early stages after the injury. In this regard, we found that inhibition of CD47 function while having no effect on VSMC apoptosis enhanced their efferocytosis *in vitro* in response to thrombin and *in vivo* in response to injury. Moreover, depletion of NFATc1 levels, the transcriptional regulator of CD47 expression, also exhibited a similar effect on rescuing VSMC efferocytosis from inhibition by thrombin. These observations imply that CD47 *via* inhibiting SMC efferocytosis may trigger paracrine mechanisms in influencing the migration and proliferation of surrounding SMCs and play a role in neointima formation. Dedifferentiation of SMCs is another characteristic feature of neointimal hyperplasia (17–19). VSMCs undergo phenotypic switching from quiescent contractile to synthetic migratory and proliferative state during vascular injury (17–19). Although both thrombin and GI induced dedifferentiation of SMCs, it appears that this phenotypic switching was independent of the involvement of CD47, as depletion of its levels or blocking its function had no effect on the downregulation of SMC contractile markers by either thrombin or GI.

Toward exploring the mechanisms involved in thrombin-induced CD47 expression, we found that its promoter contains several binding sites for NFATs and that downregulation of NFATc1 levels reduced both thrombin and GI-induced CD47 expression. Previously, we reported that PAR1-Gαq/11-PLCβ3 signaling mediates NFATc1 activation in thrombin-induced IL-33 and CDC6 expression in the modulation of VSMC migration and proliferation leading to injury-induced neointima formation (21–23). The present findings also show the involvement of PAR1-Gαq/11-PLCβ3 signaling upstream to NFATc1 activation in the induction of CD47 expression. Thus, these observations reveal that CD47 is another target of PAR1-Gαq/11-PLCβ3-NFATc1 signaling in the regulation of neointimal hyperplasia. Many studies have reported that CD47 *via* inhibiting efferocytosis plays a role in atherosclerosis (7–11). Furthermore, besides macrophages, VSMCs can also transform into foam cells and contribute to the progression of atherosclerotic lesions (23, 58–60). In this regard, our current observations show that CD47 besides inhibiting SMC efferocytosis also promotes their migration and proliferation. In view of these observations, one could infer that CD47's role in atherosclerosis may not only depend on its effects in the inhibition of efferocytosis but also may rest on its involvement in promoting VSMC migration and proliferation. In conclusion, as depicted in Figure 8, the present observations reveal that CD47 *via* inhibiting SMC efferocytosis and enhancing their migration and proliferation contributes to neointimal hyperplasia.

Experimental procedures

Materials

Anti-β-Actin (SC-47778), anti-CD47 (SC-12730), anti-E2F1 (SC-251), anti-MEK1 (SC-219), anti-p21Cip1 (SC-6246), anti-p27Kip1 (SC-528), anti-p53 (SC-6243), anti-p57Kip2 (SC-1040), and anti-PLCβ3 (SC-403) antibodies were obtained from Santa Cruz Biotechnology. Anti-Gαq (ab210004), anti-Gα11 (ab153951), anti-Integrin αV (ab179475), anti-Integrin β3 (ab119992), anti-Integrin β3 p-Y773 (ab38460), anti-Integrin β3 p-Y785 (ab190735), anti-Ki67 (ab15580), anti-LMCD1 (ab179454), anti-proteasome 20α+β (ab22673), anti-SM22α (ab14106), and anti-αSMA (ab5694) antibodies, and TUNEL Assay kit (ab66110) were bought from Abcam . Anti-SIRPα (D163M) antibody was purchased from Cell Signaling Technology. Duolink *in situ* PLA kit (DUO92101), monoclonal anti-mouse SMCα-actin antibody (A2547), and Trypan Blue solution (T8154) were obtained from Sigma-Aldrich. PCR Master Mix (M750B) was purchased from Promega. Human Gαq siRNA (ON-TARGETplus SMARTpool J-008562), human Gα11 siRNA (ON-TARGETplus SMARTpool J-010860), and control nontargeting siRNA (D-001810-10) were obtained from Dharmacon RNAi Technologies. Anti-NFATc1 (MA3-024), anti-SMMHC (21404-1-AP), anti-integrin β3 (14-0611-85), anti-SIRPα (25-1721-80), and anti-Thrombospondin1 (MA5-13398) neutralizing antibodies, goat anti-rabbit horseradish peroxidase (HRP) (31460) and goat anti-mouse HRP (31437) antibodies, human CD47 siRNA (s2684), human E2F1 siRNA (s4405), human LMCD1 siRNA (s26868), human NFATc1 siRNA (s9470), human PAR1 siRNA (s4922), human PLCβ3 siRNA (s10619) and mouse NFATc1 siRNA (MSS275980), Ibidi culture-inserts (80,206), Lipofectamine 3000 transfection reagent (L3000-015), medium 231 (M231-500), PowerUp SYBR Green Master Mix (A25780), smooth

same as in panels *B* except that cells were immunostained for integrin β3 (*green*) and CD47 (*red*) using their specific antibodies (*C*) or subjected to PLA (*D*). The n is three for panel *C* and *D*. *E–H*, quiescent HASMCs that were preincubated with IgG isotype control or indicated neutralizing antibody (10 μg/ml) were tested for thrombin (0.5 U/ml)-induced migration (*E*) and proliferation (*F–H*). The n is three for panels *E–H*. The bar graph shows Mean ± SD values of three independent experiments. *$p < 0.01$ *versus* vehicle or IgG + vehicle; **$p < 0.01$ *versus* IgG + Thrombin. nAb, neutralizing antibody. The scale bars in panels *C* and *D* represent 50 μm and 20 μm, respectively. The scale for panel *E* is 1000 μm from the extreme left to the extreme right for each image. CD47, cluster of differentiation 47; HASMC, human aortic smooth muscle cell; PLA, proximity ligation assay.

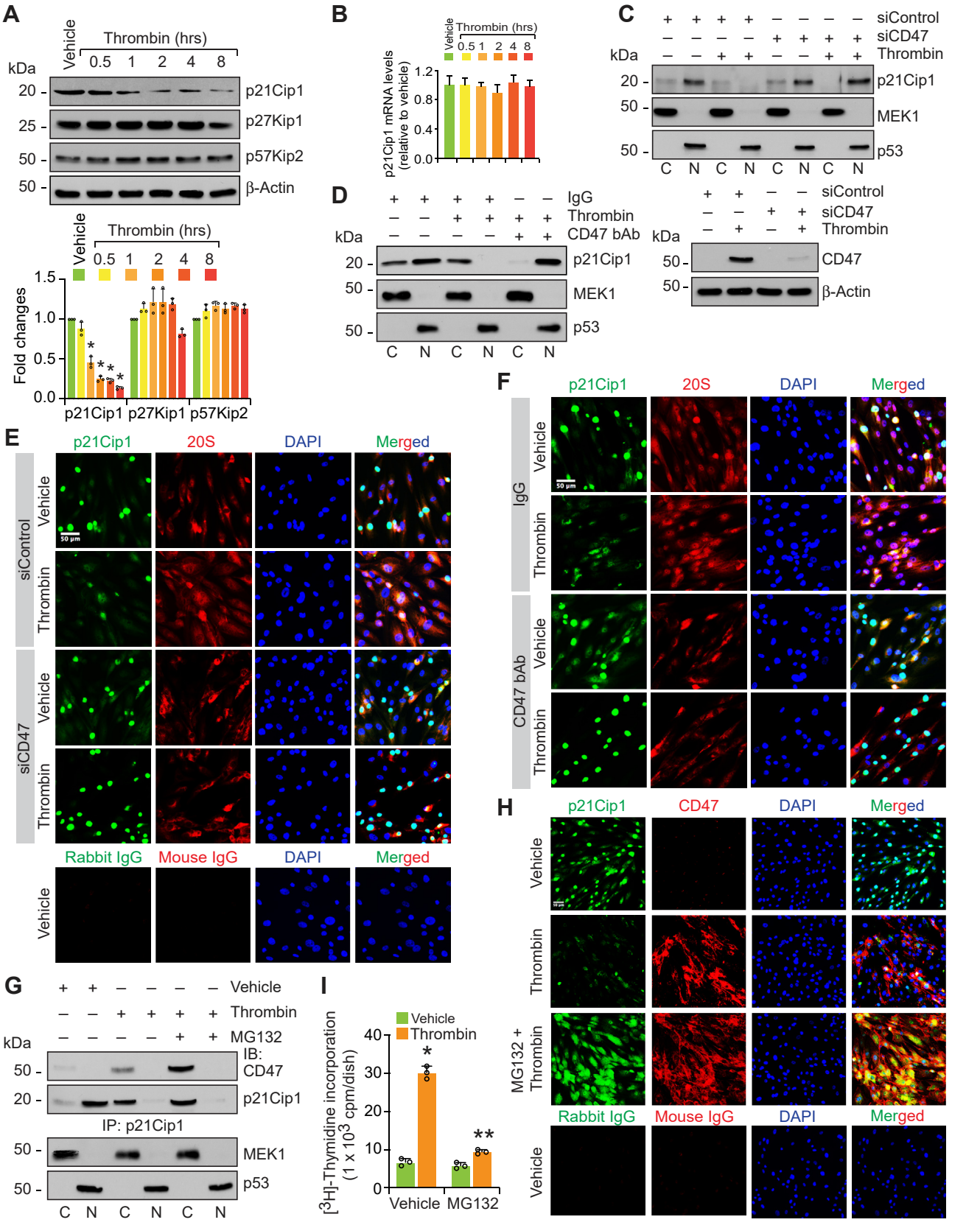

Figure 4. CD47 mediates thrombin-induced HASMC proliferation *via* facilitating p21Cip1 nuclear export and its degradation in the cytoplasm. *A*, quiescent HASMCs were treated with and without thrombin (0.5 U/ml) for the indicated time periods, cell extracts were prepared and analyzed by Western blotting for the indicated proteins using their specific antibodies. The n is three for panel *A*. *B*, all the conditions were the same as in panel *A* except that total cellular RNA was isolated and analyzed by qRT-PCR for p21Cip1 mRNA levels using its specific primers. *C* and *D*, HASMCs that were transfected with 100 nmoles of siControl or siCD47 (*C*) or preincubated (30 min) with 10 μg/ml of IgG isotype control or CD47 bAb (*D*) were treated with and without

muscle growth supplements (S-007-25), and gentamicin/amphotericin solution (R-015-10) were bought from Thermo Fisher Scientific. Enhanced chemiluminescence Western blotting detection reagents (RPN2106) were purchased from GE Healthcare. Anti-human CD47 bAb (BE0019-1), anti-mouse CD47 bAb (BE0270), and IgG isotype control antibodies (BP0083, BP0091, and BE0089) were obtained from BioXcell. Human endothelin-1 (1160) was purchased from R&D Systems. All the primers used for qRT-PCR were synthesized by IDT.

Animals

All the experiments involving animals were performed according to the guidelines of the Institutional Animal Care and Use Committee of the University of Tennessee Health Science Center and in compliance with the Guide for the Care and Use of Animals published by the NIH (Publication No. 85-23, revised 1985). C57BL/6J mice (both male and female) were obtained from The Jackson Laboratory and maintained at the University of Tennessee Health Science Center's animal facilities. The University of Tennessee Health Science Center's LACU facility maintains a 12/12 h light/dark cycle and the animals have ad libitum access to food and water. Furthermore, the animals were maintained on Teklad Irradiated LM-485 mouse/rat diet (Envigo, Catalog number 7912) and Shepherd's Cob + Plus bedding.

Ethics statement

All the experiments involving animals were approved by the Institutional Animal Care and Use Committee of the University of Tennessee Health Science Center and in compliance with the Guide for the Care and Use of Animals published by the NIH (Publication No. 85-23, revised 1985).

Cell culture

Human aortic SMCs (HASMCs) that were originated from normal human descending aorta were obtained from Cell systems (Catalog No. ACBRI 716) and subcultured at 6×10^3 cells/cm^2 in medium 231 containing growth supplements and Gentamicin/Amphotericin. MASMCs that were isolated from aorta of pathogen-free C57BL/6 mice were purchased from Cell Biologics (Catalog No. C57-6080) and subcultured at 6×10^3 cells/cm^2 in Dulbecco's modified Eagle's medium (DMEM) with 10% FBS and Pen Strep (100 U/100 μg/ml). Cultures were maintained in a humidified 95% air and 5% CO_2 atmosphere at 37 °C. Both HASMCs and MASMCs of different batches and passages between 5 and 10 were growth-arrested overnight in medium 231 or DMEM, respectively, without any growth supplements or serum and used for the experiments unless otherwise indicated.

In vitro *efferocytosis assay*

Target cells (HASMCs) were plated in 96-well microplate at a density of 1×10^5 cells/well, quiesced, and labeled with 2.5 μM carboxyfluorescein succinimidyl ester (CFSE) for 30 min at 37 °C according to the manufacturer's protocol (Invitrogen). Unincorporated CFSE was removed by quenching the cells with culture media. Effector cells (THP1-macrophages) were prepared by incubating in RPMI medium containing 150 nM phorbol 12-myristate 13-acetate for 24 h at 37 °C. Then, the labeled HASMCs were treated with and without thrombin (0.5 U/ml) for 2 h, washed with PBS, overlaid with ∼50,000 phorbol 12-myristate 13-acetate differentiated THP1-macrophages and coincubated for 2 h in serum-free medium. THP1-macrophages were then collected by aspirating the media followed by centrifugation, washed with PBS 3 times, resuspended in PBS, and the fluorescence intensity was measured at 517 nm excitation and 495 nm emission using SpectraMax Gemini XPS spectrofluorometer (Molecular Devices). STS (1 μM) was used as a positive control for the induction of efferocytosis. To test the effect of CD47 bAb on HASMC efferocytosis, quiescent HASMCs were pretreated with isotype control lgG or CD47 bAb (10 μg/ml) for 30 min, labeled with CFSE, treated with and without thrombin (0.5 U/ml) for 2 h and subjected to efferocytosis assay as described above. To test the role of NFATc1 in thrombin-induced inhibition of HASMCs efferocytosis, cells were transfected with siControl or siNFATc1 (100 nmoles), labeled with CFSE, treated with and without thrombin (0.5 U/ml) for 2 h and subjected to efferocytosis assay as described above.

Apoptosis

Apoptosis was measured using TUNEL assay kit from Abcam (ab66110) following the manufacturer's instructions.

Cell migration assay

Cell migration was measured by scratch wound assay as described by us (23). Briefly, 80 μl of medium 231 (for HASMCs) or DMEM (for MASMCs) with growth supplements containing 2×10^5 cells was added to each chamber of ibidi culture inserts and grown to confluence. After overnight growth-arrest, cells were preincubated with 10 μg/ml of blocking/neutralizing antibody or appropriate isotype control IgG for 30 min and then treated with and without thrombin

thrombin (0.5 U/ml) for 2 h, nuclear and cytoplasmic extracts were prepared and analyzed by Western blotting for the indicated proteins using their specific antibodies. *E* and *F*, all the conditions were the same as in panels *C* and *D* except that cells were immunostained for p21Cip1 (*green*) and 20Sα/β (*red*) using their specific antibodies. The n is three for panels *E* and *F*. *G*, quiescent HASMCs were treated with and without thrombin (0.5 U/ml) in the presence or absence of MG132 (10 μM) for 2 h and nuclear and cytoplasmic extracts were prepared, immunoprecipitated with p21Cip1 antibody, and the immunocomplexes were analyzed by Western blotting for the indicated proteins using their specific antibodies. *H*, all the conditions were the same as in panel *G* except that cells were fixed and stained for p21Cip1 (*green*) and CD47 (*red*) using their specific antibodies. The n is three for panel *H*. *I*, quiescent HASMCs were treated with and without thrombin (0.5 U/ml) in the presence or absence of MG132 (10 μM) for 2 h and subjected for proliferation assay. The n is three for panel *I*. The bar graph shows Mean ± SD values of three independent experiments. *$p < 0.01$ *versus* vehicle; **$p < 0.01$ *versus* Thrombin. The scale bars in panels *E–H* represent 50 μm. bAb, blocking antibody; CD47, cluster of differentiation 47; Cip1, CDK-interacting protein 1; HASMC, human aortic smooth muscle cell.

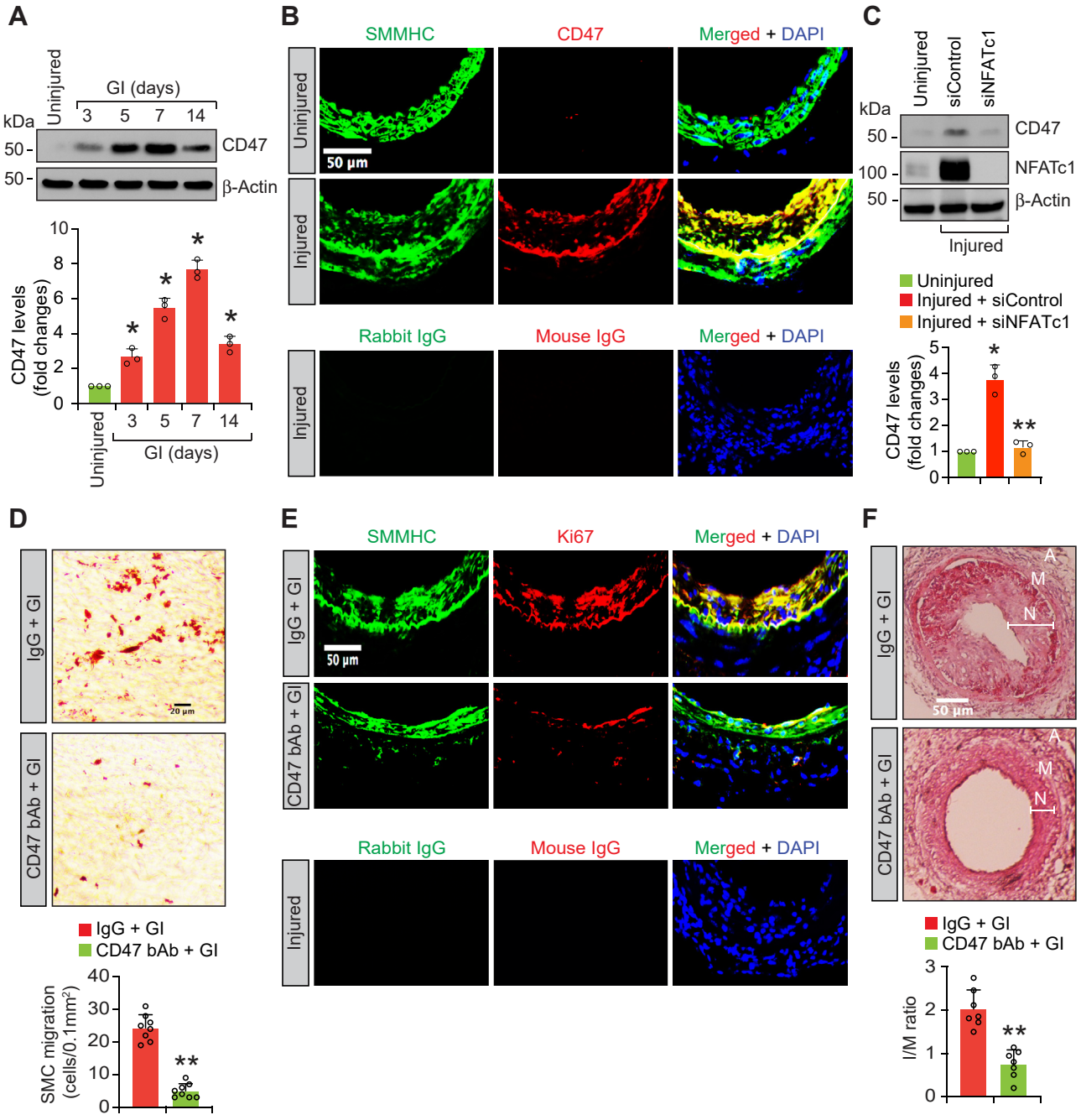

Figure 5. Blocking CD47 function mitigates injury-induced neointimal hyperplasia. *A*, tissue extracts prepared from uninjured and various time periods of post guide wire-injured (GI) mouse femoral arteries were analyzed by Western blotting for CD47 levels using its specific antibodies and the blot was normalized to β-actin levels. The n is three for panel *A*. *B*, double immunofluorescence staining of uninjured and injured artery cross sections for SMMHC (*green*) and CD47 (*red*). Injured artery cross sections were also stained with mouse or rabbit IgGs as negative controls. The n is seven for panel *B*. *C*, an equal amount of protein from 3 days of post-GI femoral arteries that received either Control or NFATc1 siRNA (10 μg/artery) or uninjured arteries were analyzed by Western blotting for CD47 levels using its specific antibody and the blot was reprobed for NFATc1 or β-actin levels to show the efficacy of the siRNA on its target and off target molecules levels. The n is three for panel *C*. *D*, femoral arteries from 5 days of post-GI mice that were administered with IgG isotype control or CD47 blocking bAb (50 μg/mouse by ip) were isolated, opened longitudinally and stained for SMMHC. The n is seven for panel *D*. The bar graph shows Mean ± SD values of the SMMHC-positive cells on the luminal surface of the femoral arteries from injured + IgG isotype control and injured + CD47 bAb administered mice (n = 7). *E* and *F*, mice were subjected to GI and administered with IgG isotype control or CD47 bAb immediately after GI and every 3 days thereafter (50 μg/mouse by ip). After 1 week and 3 weeks of post-GI, mice were sacrificed, femoral arteries were isolated, fixed, and cross-sections were prepared. The artery sections of 1 week post-GI mice were coimmunostained for SMMHC and Ki67 (*E*), whereas the artery sections of 3 weeks of post-GI mice were stained with H&E and the I/M ratios were calculated (*F*). The n is seven for panels *E* and *F*. The bar graph shows Mean ± SD values of the I/M ratios of the femoral arteries from injured + IgG isotype control and injured + CD47 bAb administered mice (n = 7). *$p < 0.01$ *versus* uninjured; **$p < 0.01$ *versus* siControl + GI or IgG + GI. The scale bars in panels *B*, *E*, and *F* represent 50 μm and panel *D* is 20 μm. bAb, blocking antibody; CD47, cluster of differentiation 47; I/M, intimal/medial; NFATc1, nuclear factor of activated T cells c1; SMMHC, smooth muscle myosin heavy chain.

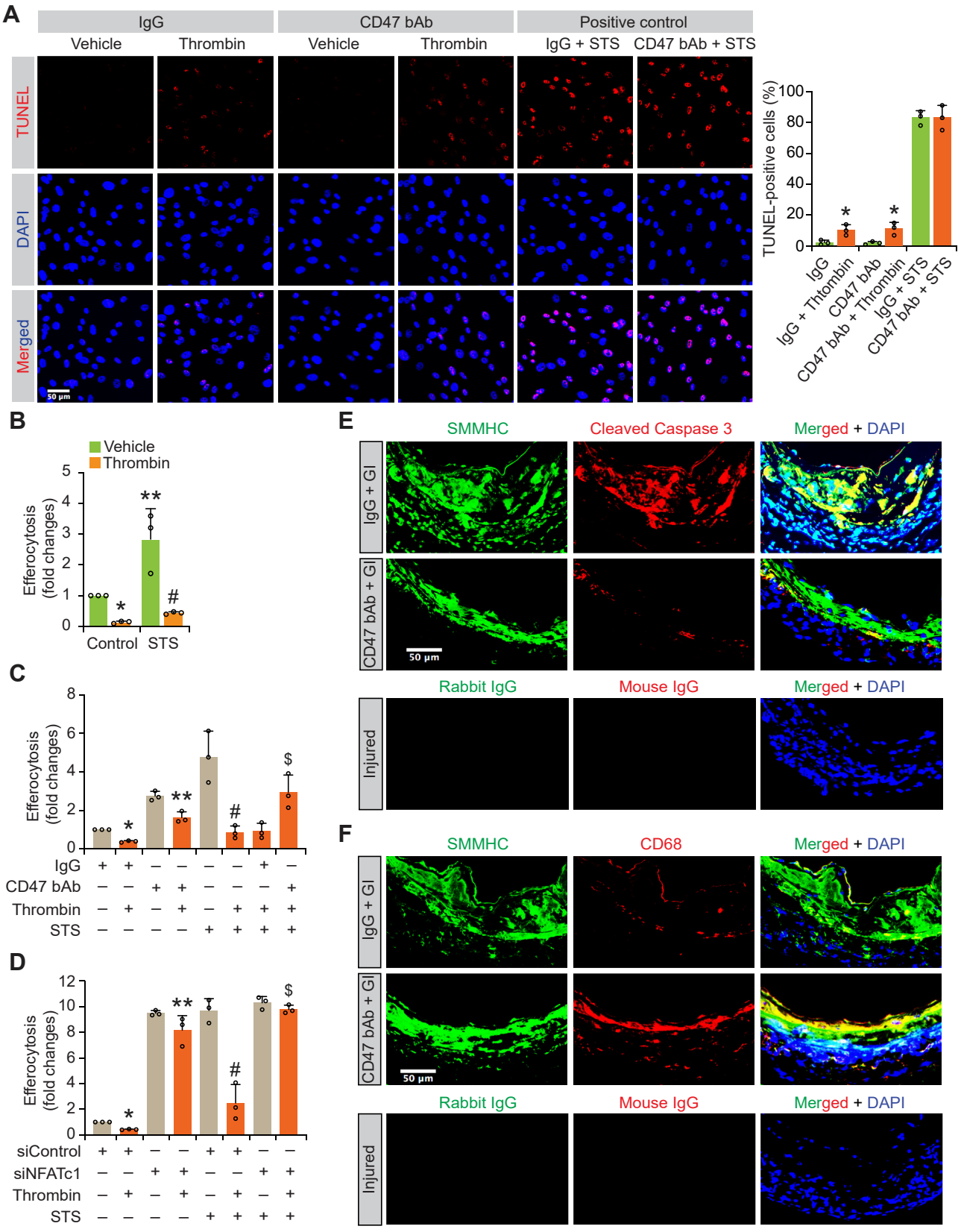

Figure 6. CD47 inhibits VSMC efferocytosis *in vitro* in response to thrombin and *in vivo* in response to injury. *A*, quiescent HASMCs that were preincubated (30 min) with IgG isotype control or CD47 bAb (10 μg/ml) were treated with and without thrombin (0.5 U/ml) for 2 h, fixed, and apoptosis was measured by TUNEL assay. STS (1 μM) was used as a positive control. The n is three for panel *A*. *B*, quiescent HASMCs were labeled with CFSE (2.5 μM), treated with and without thrombin (0.5 U/ml) for 2 h, washed with PBS, overlaid with PMA differentiated THP1-macrophages, and coincubated for 2 h in serum-free medium. THP1-macrophages were then collected, washed with PBS, and the fluorescence intensity was measured at 517 nm excitation and 495 nm emission. STS (1 μM) was used as a positive control for induction of apoptosis. The n is three for panel *B*. *C*, quiescent HASMCs that were pretreated

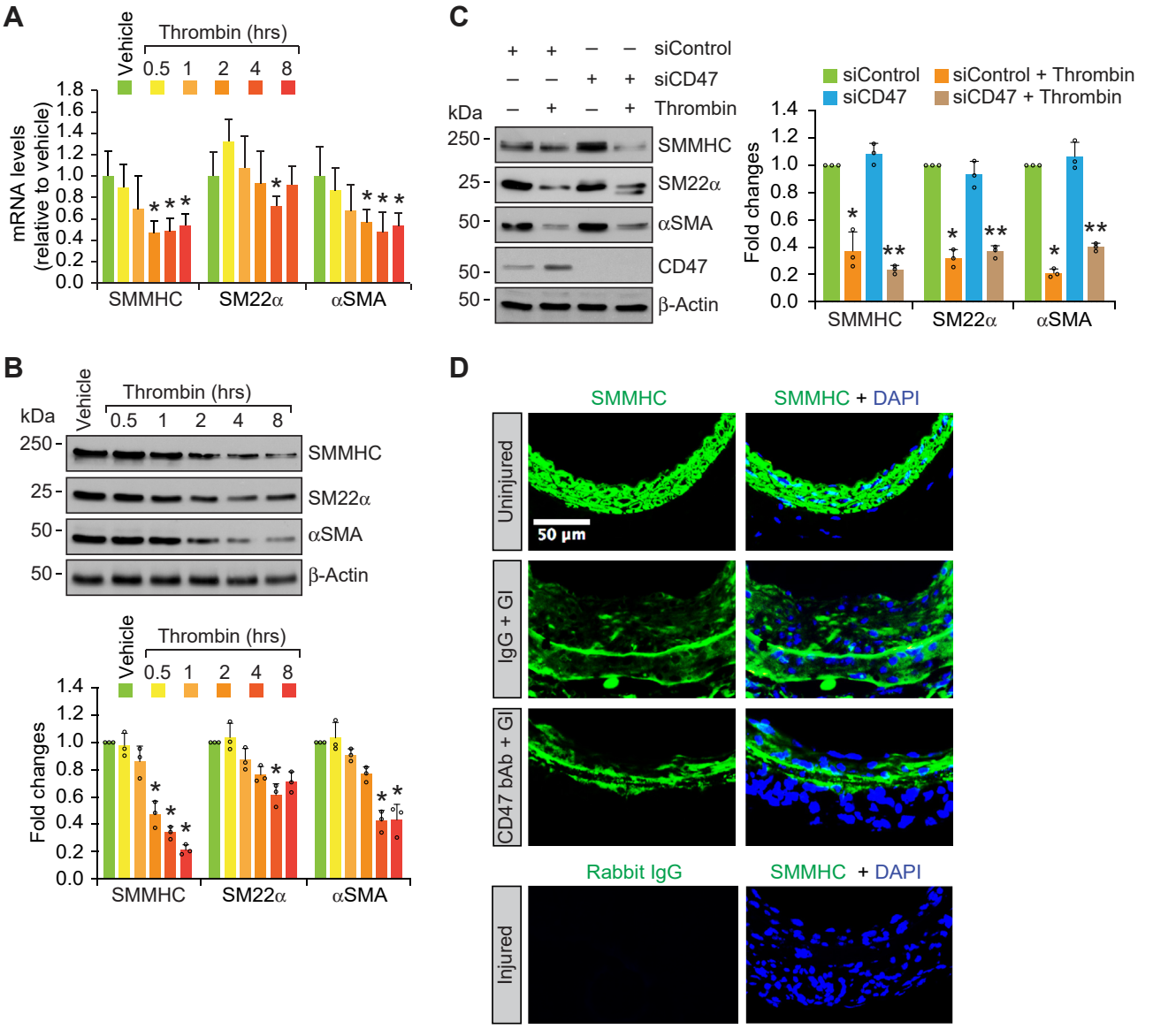

Figure 7. Lack of a role for CD47 in VSMC dedifferentiation. *A* and *B*, quiescent HASMCs were treated with and without thrombin (0.5 U/ml) for the indicated time periods, either RNA was isolated and analyzed by qRT-PCR for mRNA levels of the indicated molecules using their specific primers (*A*) or cell extracts were prepared and analyzed by Western blotting for the expression levels of the indicated proteins using their specific antibodies (*B*). The n is three for panels *A* and *B*. *C*, HASMCs were transfected with the siControl or siCD47 (100 nmoles), quiesced, treated with and without thrombin (0.5 U/ml) for 2 h, cell extracts were prepared and analyzed by Western blotting for the expression levels of the indicated proteins using their specific antibodies. The n is three for panel *C*. *D*, double immunofluorescence staining of cross sections from uninjured and 3 weeks of post-GI arteries of mice that received IgG isotype control or CD47 blocking bAb (50 μg/mouse by ip) for SMMHC. Injured artery cross sections were also stained with appropriate control IgGs as negative controls. The n is seven for panel *D*. The bar graph shows Mean ± SD values of three independent experiments. *$p < 0.01$ *versus* vehicle or siControl + vehicle; **$p < 0.01$ *versus* siCD47 + vehicle. The scale bar in panel *D* represents 50 μm. bAb, blocking antibody; CD47, cluster of differentiation 47; GI, guidewire injury; HASMC, human aortic smooth muscle cell; SMMHC, smooth muscle myosin heavy chain; VSMC, vascular smooth muscle cell.

(0.5 U/ml) in the presence of 5 mM hydroxyurea for 24 h. The details of blocking/neutralizing antibodies (bAb/nAb) and their isotype control IgGs used in present study are as follows: Human CD47 bAb (Cat # BE0019-1; clone B6.H12; mouse IgG1, κ) and its isotype control IgG (Cat # BP0083; clone MOPC-21; mouse IgG1, κ). Mouse CD47 bAb (Cat # BE0270;

with IgG isotype control or CD47 bAb (10 μg/ml) for 30 min were labeled with CFSE, treated with and without thrombin (0.5 U/ml) for 2 h, and subjected to efferocytosis assay as described in panel *B*. The n is three for panel *C*. *D*, HASMCs that were transfected with siControl or siNFATc1 were labeled with CFSE, treated with and without thrombin (0.5 U/ml) for 2 h, and subjected to efferocytosis assay as described in panel *B*. The n is three for panel *D*. *E* and *F*, mice were subjected to GI and administered with IgG isotype control or CD47 bAb immediately after GI and every 3 days thereafter (50 μg/mouse by ip). After 3 weeks of post-GI, mice were sacrificed, femoral arteries were isolated, fixed, and cross-sections were prepared. The artery sections were coimmunostained for SMMHC and cleaved caspase 3 (*E*) or SMMHC and CD68 (*F*). The n is seven for panels *E* and *F*. The bar graphs represent Mean ± SD values of three independent experiments. *$p < 0.01$ *versus* vehicle or IgG + vehicle or siControl + vehicle; **$p < 0.01$ *versus* Thrombin or IgG + Thrombin or siControl + Thrombin; $^{\#}p < 0.01$ *versus* STS or siControl + STS; $^{\$}p < 0.01$ *versus* IgG + STS + Thrombin or siControl + STS + Thrombin. The scale bars in panels *A*, *E*, and *F* represent 50 μm. CD47, cluster of differentiation 47; CFSE, carboxyfluorescein succinimidyl ester; GI, guidewire injury; HASMC, human aortic smooth muscle cell; PMA, phorbol 12-myristate 13-acetate; STS, staurosporine; VSMC, vascular smooth muscle cell.

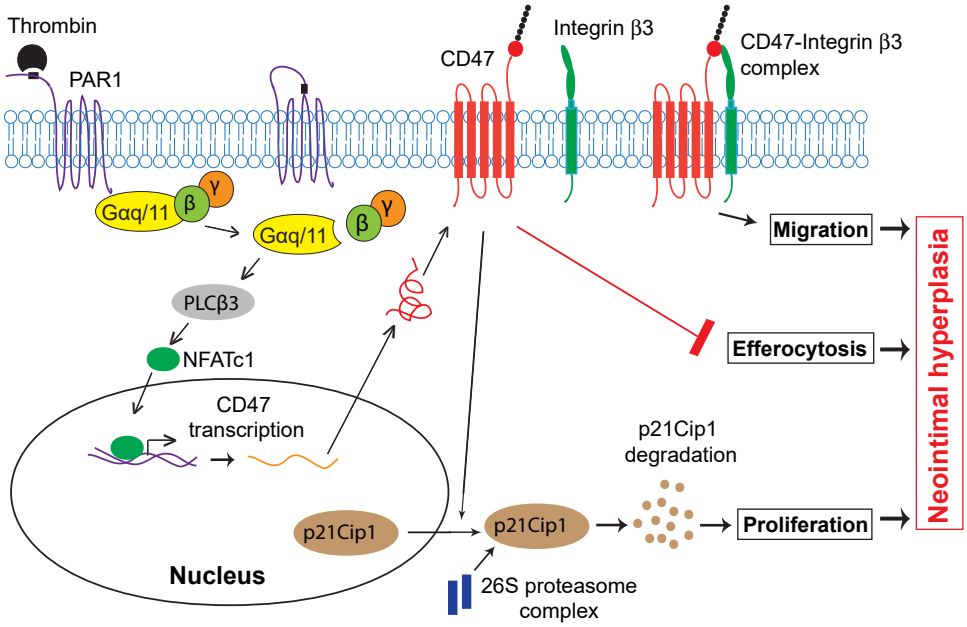

Figure 8. Schematic diagram depicting the overall signaling of CD47 role in neointimal hyperplasia.

clone MIAP301; Rat IgG2a, κ) and its isotype control IgG (Cat # BE0089; clone 2A3; Rat IgG2a, κ). Human integrin β3 nAb (Cat # 14-0611-85; clone 2C9.G3; American hamster IgG) and its isotype control IgG (Cat # BP0091; clone N/A; American hamster IgG). Human TSP1 nAb (Cat # MA5-13398; clone A6.1; Mouse IgG1, κ) and its isotype control IgG (Cat # BP0083; clone MOPC-21; mouse IgG1, κ). Human SIRPα nAb (Cat # 25-1721-80; clone p84; Rat IgG1, κ) and its isotype control IgG (Cat # BE0088; clone HRPN; Rat IgG1, κ). Hydroxyurea is an inhibitor of ribonucleotide reductase and therefore prevents replicative DNA synthesis and arrests cells in the S-phase of the cycle (61). After 24 h, cells were observed under Nikon Eclipse TS100 microscope with 10×/0.25 magnification before and after the experimental period and images were captured with charge-coupled device color camera (KP-D20AU) by using Apple iMovie 7.1.4 software (https://support.apple.com/kb/dl13?locale=en_US). HASMC migration was expressed as percentage of wound closure (total wound area at 0 h, wound area at 24 h/total area at 0 h × 100).

DNA synthesis assay

HASMC and MASMC DNA synthesis was measured by [^{3}H]-thymidine incorporation as described by us and expressed as counts per min per dish (24).

Quantitative RT-PCR

Total cellular RNA was isolated from HASMCs and MASMCs with appropriate treatments using TRIzol reagent as per the manufacturer's instructions. RT was performed with a High-Capacity cDNA RT Kit (Applied Biosystems). Quantitative reverse transcriptase-PCR (qRT-PCR) was then performed on a 7300 Real-Time PCR system (Applied Biosystems) using SYBR Green Master Mix (Applied Biosystems) as per the manufacturer's instructions. Beta actin was used as endogenous control. The PCR amplifications were performed on a 7300 Real-Time PCR system operated with SDS version 1.4 program (https://www.thermofisher.com/order/catalog/product/4379633) and Delta Rn analysis method (Applied Biosystems). All the primers used for qRT-PCR in this study were synthesized by IDT and listed in Table 1.

Coimmunoprecipitation

Cells extracts were prepared by lysis in 400 μl of lysis buffer (PBS, 1% Nonidet P40, 0.5% sodium deoxycholate, 0.1% SDS, 100 μg/ml PMSF, 100 μg/ml aprotinin, 1 μg/ml leupeptin, and 1 mM sodium orthovanadate) for 20 min on ice. The extracts were cleared by centrifugation at 12,000 rpm for 20 min at 4 °C. The cleared cell extracts containing an equal amount of

Table 1
Primers used for qRT-PCR

Gene	Forward primer 5′ → 3′	Reverse primer 5′ → 3′
Human CD47	CCTGCAGCACTTTTTCCTTC	CAAGAGCGAACCCCAAATAA
Human p21Cip1	GACACCACTGGAGGGTGACT	CAGGTCCACATGGTCTTCCT
Human SMMHC	AACACCTGCCCATCTACTCG	ACGGCCAGGTACTGAATGAC
Human SM22α	AAGAATGATGGGCACTACCG	ACTGATGATCTGCCGAGGTC
Human αSMA	AGAACATGGCATCATCACCA	TACATGGCTGGGACATTGAA
Human β-actin	AGCCATGTACGTTGCTAT	GATGTCCACGTCACACTTCA
Mouse CD47	TAGCACTACTACAGATCAAA	CACCATGGCATCGCGCTTAT
Mouse β-actin	AGCCATGTACGTAGCCATCC	CTCTCAGCTGTGGTGGTGAA

Abbreviations: αSMA, αsmooth muscle actin; CD47, cluster of differentiation 47; Cip1, CDK-interacting protein 1; SM22 α; smooth muscle 22α; SMMHC, smooth muscle myosin heavy chain.

protein (400 μg) from control and the indicated treatments were incubated with the indicated antibodies (4 μg) overnight at 4 °C, followed by incubation with protein A/G-Sepharose CL4B beads for 3 h with gentle rocking. The beads were collected by centrifugation at 1000 rpm for 2 min at 4 °C and washed 4× with lysis buffer and once with PBS. The immunocomplexes were released by heating the beads in 40 μl of Laemmli sample buffer and analyzed by Western blotting for the indicated molecules using their specific antibodies.

Western blotting

Cells with and without appropriate treatments were scraped into RIPA buffer (PBS containing 1% Nonidet P40, 0.5% sodium deoxycholate, 0.1% SDS, 100 μg/ml PMSF, 100 μg/ml aprotinin, 1 μg/ml leupeptin, and 1 mM sodium orthovanadate) and lysed by sonication at 45% amplitude for 15 s with 10 s intervals for 2 min on ice (Branson Sonifier 450). To prepare aortic extracts, it was chopped and minced in RIPA buffer and homogenized by sonication at 45% amplitude for 15 s with 10 s intervals for 4 min on ice. Cell or tissue extracts were cleared by centrifugation at 12,000 rpm for 10 min at 4 °C and protein concentration was determined using Mico BCA kit (Thermo Fisher Scientific). Cell or tissue extracts containing equal amounts of protein from control and the indicated treatments were resolved by electrophoresis on 0.1% (w/v) SDS and 10% or 12% (w/v) polyacrylamide gels. The proteins were transferred electrophoretically onto a nitrocellulose membrane. After blocking in 5% (w/v) nonfat dry milk or 5% BSA, the membranes were incubated with the appropriate primary antibodies at 1:1000 dilution overnight at 4 °C, followed by incubation with horseradish peroxidase-conjugated secondary antibodies at 1:5000 dilution for 1 h at RT. After washing in Tris buffered saline containing Tween 20 three times, the membranes were incubated with enhanced chemiluminescence detection reagent to detect antigen-antibody complexes. The band intensities were quantified by densitometry using NIH ImageJ 1.49v software (http://imagej.nih.gov/ij).

Transfections

HASMCs and MASMCs were transfected with nontargeted or on-targeted siRNA at a final concentration of 100 nmol using Lipofectamine 3000 transfection reagent as per the manufacturer's instructions. After 6 h of transfection, cells were recovered in complete medium for 24 h, growth-arrested overnight in serum-free medium and used as required.

Trypan blue exclusion assay

Cells 36 h after transfection with siControl or target siRNA were examined for viability by Trypan blue exclusion assay as per the manufacturer's (Sigma-Aldrich) instructions.

Guidewire injury

Mice were anesthetized by single intraperitoneal injection of ketamine (80 mg/kg body weight)/xylazine (6 mg/kg body weight) and subjected to GI as described by us (23, 24). The left femoral artery was exposed by blunted dissection. Both the vein and artery were looped together proximally and distally with 4 to 0 silk sutures for blood flow control during the procedure. A small muscular branch of the femoral artery was isolated and a small incision was made on this exposed muscular branch and a straight spring wire (0.38 mm in diameter, No. C-SF-15-15, COOK) was inserted into the lumen of the femoral artery. The wire was moved back and forth 2 times to denude the artery. After removal of the spring wire, the muscular branch of the artery was ligated. Releasing the sutures that were placed in the proximal and distal femoral portions restored the blood flow in the injured femoral artery. To downregulate NFATc1 levels in the femoral arteries, control (Cat # D-001810-10) or NFATc1 siRNA (Cat # MSS275980) was premixed with Invivofectamine 3.0, then suspended in 30% Pluronic gel (10 μg siRNA in 100 μl of Pluronic gel) and applied perivascularly around the injured arteries as described (23). The skin incision was closed using sutures. The Pluronic gel solidifies on contact with tissue and forms a gel, which ensures sustained release of siRNA. At the indicated time periods of post-GI, the animals were euthanized by single intraperitoneal injection of ketamine (160 mg/kg body weight)/xylazine (12 mg/kg body weight) and femoral arteries were carefully dissected out. The arteries were used to prepare tissue extracts for Western blot analysis or fixed overnight in 4% paraformaldehyde (PFA) in PBS at 4 °C to make artery sections. After fixing in PFA, the arteries were incubated overnight in 30% sucrose at 4 °C, embedded in optimal cutting temperature compound and 5 μm-thick sections were cut in the middle of the artery. The sections were stained with H&E to measure neointimal growth or coimmuostained for CD47 or Ki67 in combination with SMMHC. The intimal (I) and medial (M) areas were measured using NIH ImageJ 1.49v software (http://imagej.nih.gov/ij), and the I/M ratios were calculated.

Injection of antibodies into mice

One day before GI, mice were injected with IgG isotype control or CD47 bAb (clone MIAP301) (50 μg by ip) and thereafter every 3 days up to 3 weeks.

In vivo *SMC migration assay*

In vivo SMC migration was measured as per the method described earlier (62). Briefly, 5 days after GI, the femoral arteries were dissected out and fixed in 4% PFA overnight at 4 °C. The middle of the injured femoral artery was cut and fixed again in cold acetone for 10 min. The artery was then opened longitudinally and pinned down onto an agar plate with the luminal surface facing up. The arteries were rinsed with PBS and treated with 3% H_2O_2 for 15 min to block the endogenous peroxidase activity. After blocking in 5% goat serum in PBS for 30 min, the arteries were incubated with anti-mouse SMMHC antibody (1:300) overnight at 4 °C, followed by incubation with biotinylated goat anti-mouse IgG for 30 min. After rinsing with PBS for 5 min, peroxidase labeling was performed using ABC kit and coverslips were placed. The luminal surface of the

artery was examined under Nikon Eclipse 50i microscope with 40×/0.25 magnification and the images were captured with Nikon Digital Sight DS-L3 color camera. SMMHC-positive cells were counted.

Immunofluorescence

After appropriate treatments, HASMCs were fixed with 3.7% PFA for 15 min, permeabilized in 0.3% Triton X100 for 15 min, blocked with 3% BSA for 1 h and incubated with the indicated antibodies (1:100 dilution) at 4 °C overnight. Then Alexa Fluor 488-conjugated goat anti-mouse and Alexa Fluor 568-conjugated goat anti-rabbit secondary antibodies were added (1:500) and incubation continued for 1 h at RT. After washing with PBS, cells were counterstained with DAPI, and mounted onto glass slides with Prolong Gold antifade mounting medium. In case of mouse femoral artery cryosections, after permeabilization with 0.5% Triton X100 for 15 min, the sections were blocked in normal goat serum for 1 h and incubated with the indicated antibodies (1:100 dilution) overnight followed by incubation with Alexa Fluor 488-conjugated goat anti-mouse and Alexa Fluor 568-conjugated goat anti-rabbit secondary antibodies (1:300 dilution). The sections were washed with PBS, counterstained with DAPI, mounted with a cover slip using Prolong Gold antifade mounting medium. The immunostained cells or sections were observed under a Zeiss Inverted Microscope (Zeiss AxioObserver Z1; Magnification at 10×/0.25 NA or 40×/0.6 NA) and the fluorescence images were captured with a Zeiss AxioCam MRm camera using the microscope operating software and Image Analysis Software Zen 2.6 (blue edition, Carl Zeiss Imaging Solutions GmbH) (https://www.zeiss.com/content/dam/Microscopy/Downloads/Pdf/zenreleasenotes/zen-2_6_blue_edition-release-notes.pdf).

Proximity ligation assay

PLA was performed as described (22). Briefly, after appropriate treatments, HASMCs were fixed with 4% PFA for 15 min, permeabilized in 0.3% Triton X100 for 15 min, and blocked with 3% BSA for 1 h. The cells were then incubated with mouse anti-CD47 (1:100) and rabbit anti-integrin β3 (1:100) antibodies overnight at 4 °C followed by incubation with goat anti-mouse secondary antibody conjugated with oligonucleotide PLA probe Plus and goat anti-rabbit secondary antibody conjugated with oligonucleotide PLA probe Minus for 1 h at 37 °C. The cells were then incubated with a ligation solution for 30 min at 37 °C followed by a rolling-circle amplification of ligated oligonucleotide probes. A fluorescently labeled complementary oligonucleotide detection probe was used to amplify the oligonucleotides conjugated to the secondary antibodies. After washing with wash buffer, the slides were mounted with a mounting media containing DAPI. PLA signals were examined using a Zeiss inverted fluorescence microscope (AxioObserver. Z1; X100/0.045NA) and the fluorescence images were captured using Zeiss AxioCam MRm camera and microscope operating image analysis software Zen 2.6 (blue edition).

Statistical analysis

All the experiments were repeated 3 times. Normality of data was checked using Anderson-Darling Normality Test and F-test was used to assess the equality and group variance. The treatment effects were analyzed by student t test for two group comparisons and one-way ANOVA followed by Bonferroni post hoc test for multiple comparisons. All the statistical tests were performed using GraphPad Prism 8.0 software (https://www.graphpad.com/features). In the case of *in vivo* experiments, a minimum of seven mice for each gender were included. Since we did not observe statistical differences between male and female mice in our experiments on neointima formation, we did not express the results separately. The data are presented as Mean ± SD and the $p < 0.05$ were considered statistically significant.

Data availability

All data are contained within the article.

Author contributions—S. G. formal analysis; S. G. writing-original draft; S. G., P.P., and R. K. investigation; G. N. R. conceptualization; G. N. R. funding acquisition; G. N. R. supervision.

Funding and additional information—This work was supported by NHLBI, National Institutes of Health Grants HL069908 and HL103575 to G. N. R. The content is solely the responsibility of the authors and does not necessarily represent the official views of the National Institutes of Health.

Conflict of interest—The authors declare that they have no conflicts of interest with the contents of this article.

Abbreviations—The abbreviations used are: αSMA, αsmooth muscle actin; bAb, blocking antibody; CD47, cluster of differentiation 47; CDC6, cell division cycle 6; CDK, cyclin-dependent kinase; CFSC, carboxyfluorescein succinimidyl ester; Cip1, CDK-interacting protein 1; DMEM, Dulbecco's modified Eagle's medium; GI, guidewire injury; HASMC, human aortic smooth muscle cell; IL-33, interleukin-33; LMCD1, LIM and cysteine-rich domains protein 1; MASMC, mouse aortic smooth muscle cell; NFATc1, nuclear factor of activated T cells c1; PAR1, protease-activated receptor 1; PFA, paraformaldehyde; PLA, proximity ligation assay; PLCβ3, phospholipase Cβ3; SIRP α, signal regulatory protein α; SM22 α, smooth muscle 22α; SMC, smooth muscle cell; SMMHC, smooth muscle myosin heavy chain; STA, staurosporine; TSP1, thrombospondin 1; VSMC, vascular smooth muscle cell.

References

1. Ebert, M. L. A., Schmidt, V. F., Pfaff, L., von Thaden, A., Kimm, M. A., and Wildgruber, M. (2021) Animal models of neointimal hyperplasia and restenosis: species-specific differences and implications for translational research. *JACC Basic Transl. Sci.* **6**, 900–917
2. Sick, E., Jeanne, A., Schneider, C., Dedieu, S., Takeda, K., and Martiny, L. (2012) CD47 update: a multifaceted actor in the tumour microenvironment of potential therapeutic interest. *Br. J. Pharmacol.* **167**, 1415–1530
3. Soto-Pantoja, D. R., Kaur, S., and Roberts, D. D. (2015) CD47 signaling pathways controlling cellular differentiation and responses to stress. *Crit. Rev. Biochem. Mol. Biol.* **50**, 212–230

4. Cham, L. B., Torrez Dulgeroff, L. B., Tal, M. C., Adomati, T., Li, F., Bhat, H., *et al.* (2020) Immunotherapeutic blockade of CD47 inhibitory signaling enhances innate and adaptive immune responses to viral infection. *Cell Rep.* **31**, 107494
5. Eladl, E., Tremblay-LeMay, R., Rastgoo, N., Musani, R., Chen, W., Liu, A., *et al.* (2020) Role of CD47 in hematological malignancies. *J. Hematol. Oncol.* **13**, 96
6. Hayat, S. M. G., Bianconi, V., Pirro, M., Jaafari, M. R., Hatamipour, M., and Sahebkar, A. (2020) CD47: role in the immune system and application to cancer therapy. *Cell Oncol. (Dordr.)* **43**, 19–30
7. Kojima, Y., Volkmer, J. P., McKenna, K., Civelek, M., Lusis, A. J., Miller, C. L., *et al.* (2016) CD47-blocking antibodies restore phagocytosis and prevent atherosclerosis. *Nature* **536**, 86–90
8. Kojima, Y., Weissman, I. L., and Leeper, N. J. (2017) The role of efferocytosis in atherosclerosis. *Circulation* **135**, 476–489
9. Egaña-Gorroño, L., Chinnasamy, P., Casimiro, I., Almonte, V. M., Parikh, D., Oliveira-Paula, G. H., *et al.* (2019) Allograft inflammatory factor-1 supports macrophage survival and efferocytosis and limits necrosis in atherosclerotic plaques. *Atherosclerosis* **289**, 184–194
10. Ye, Z. M., Yang, S., Xia, Y. P., Hu, R. T., Chen, S., Li, B. W., *et al.* (2019) LncRNA MIAT sponges miR-149-5p to inhibit efferocytosis in advanced atherosclerosis through CD47 upregulation. *Cell Death Dis.* **10**, 138
11. Mueller, P. A., Kojima, Y., Huynh, K. T., Maldonado, R. A., Ye, J., Tavori, H., *et al.* (2022) Macrophage LRP1 (Low-Density lipoprotein receptor-related protein 1) is required for the effect of CD47 blockade on efferocytosis and atherogenesis-brief report. *Arterioscler. Thromb. Vasc. Biol.* **42**, e1–e9
12. Dou, M., Chen, Y., Hu, J., Ma, D., and Xing, Y. (2020) Recent advancements in CD47 signal transduction pathways involved in vascular diseases. *Biomed. Res. Int.* **2020**, 4749135
13. Isenberg, J. S., Roberts, D. D., and Frazier, W. A. (2008) CD47: a new target in cardiovascular therapy. *Arterioscler. Thromb. Vasc. Biol.* **28**, 615–621
14. Sajid, M., Hu, Z., Guo, H., Li, H., and Stouffer, G. A. (2001) Vascular expression of integrin-associated protein and thrombospondin increase after mechanical injury. *J. Investig. Med.* **49**, 398–406
15. Slee, J. B., Alferiev, I. S., Nagaswami, C., Weisel, J. W., Levy, R. J., Fishbein, I., *et al.* (2016) Enhanced biocompatibility of CD47-functionalized vascular stents. *Biomaterials* **87**, 82–92
16. Inamdar, V. V., Fitzpatrick, E., Alferiev, I., Nagaswami, C., Spruce, L. A., Fazelinia, H., *et al.* (2020) Stability and bioactivity of pepCD47 attachment on stainless steel surfaces. *Acta Biomater.* **104**, 231–240
17. Goel, S. A., Guo, L. W., Liu, B., and Kent, K. C. (2012) Mechanisms of post-intervention arterial remodelling. *Cardiovasc. Res.* **96**, 363–371
18. Schwartz, S. M., deBlois, D., and O'Brien, E. R. (1995) The intima. Soil for atherosclerosis and restenosis. *Circ. Res.* **77**, 445–465
19. Marx, S. O., Totary-Jain, H., and Marks, A. R. (2011) Vascular smooth muscle cell proliferation in restenosis. *Circ. Cardiovasc. Interv.* **4**, 104–111
20. Lacolley, P., Regnault, V., Nicoletti, A., Li, Z., and Michel, J. B. (2012) The vascular smooth muscle cell in arterial pathology: a cell that can take on multiple roles. *Cardiovasc. Res.* **95**, 194–204
21. Gallo, R., Padurean, A., Toschi, V., Bichler, J., Fallon, J. T., Chesebro, J. H., *et al.* (1998) Prolonged thrombin inhibition reduces restenosis after balloon angioplasty in porcine coronary arteries. *Circulation* **97**, 581–588
22. Janjanam, J., Zhang, B., Mani, A. M., Singh, N. K., Traylor, J. G., Jr., Orr, A. W., *et al.* (2018) LIM and cysteine-rich domains 1 is required for thrombin-induced smooth muscle cell proliferation and promotes atherogenesis. *J. Biol. Chem.* **293**, 3088–3103
23. Govatati, S., Pichavaram, P., Janjanam, J., Zhang, B., Singh, N. K., Mani, A. M., *et al.* (2019) NFATc1-E2F1-LMCD1-Mediated IL-33 expression by thrombin 1s required for injury-induced neointima formation. *Arterioscler. Thromb. Vasc. Biol.* **39**, 1212–1226
24. Govatati, S., Pichavaram, P., Janjanam, J., Guo, L., Virmani, R., and Rao, G. N. (2020) Myristoylation of LMCD1 leads to its species-specific derepression of E2F1 and NFATc1 in the modulation of CDC6 and IL-33 expression during development of vascular lesions. *Arterioscler. Thromb. Vasc. Biol.* **40**, 1256–1274
25. Boro, M., Govatati, S., Kumar, R., Singh, N. K., Pichavaram, P., Traylor, J. G., Jr., *et al.* (2021) Thrombin-Par1 signaling axis disrupts COP9 signalosome subunit 3-mediated ABCA1 stabilization in inducing foam cell formation and atherogenesis. *Cell Death Differ.* **28**, 780–798
26. Kawamura, T., Ono, K., Morimoto, T., Akao, M., Iwai-Kanai, E., Wada, H., *et al.* (2004) Endothelin-1-dependent nuclear factor of activated T lymphocyte signaling associates with transcriptional coactivator p300 in the activation of the B cell leukemia-2 promoter in cardiac myocytes. *Circ. Res.* **94**, 1492–1499
27. Ivey, K., Tyson, B., Ukidwe, P., McFadden, D. G., Levi, G., Olson, E. N., *et al.* (2003) Galphaq and Galpha11 proteins mediate endothelin-1 signaling in neural crest-derived pharyngeal arch mesenchyme. *Dev. Biol.* **255**, 230–237
28. Brown, E. J., and Frazier, W. A. (2001) Integrin-associated protein (CD47) and its ligands. *Trends Cell Biol.* **11**, 130–135
29. Barazi, H. O., Li, Z., Cashel, J. A., Krutzsch, H. C., Annis, D. S., Mosher, D. F., *et al.* (2002) Regulation of integrin function by CD47 ligands. Differential effects on alpha vbeta 3 and alpha 4beta1 integrin-mediated adhesion. *J. Biol. Chem.* **277**, 42859–42866
30. Matozaki, T., Murata, Y., Okazawa, H., and Ohnishi, H. (2009) Functions and molecular mechanisms of the CD47-SIRPalpha signalling pathway. *Trends Cell Biol.* **19**, 72–80
31. Barclay, A. N., and Van den Berg, T. K. (2014) The interaction between signal regulatory protein alpha (SIRPα) and CD47: structure, function, and therapeutic target. *Annu. Rev. Immunol.* **32**, 25–50
32. Israeli-Rosenberg, S., Manso, A. M., Okada, H., and Ross, R. S. (2014) Integrins and integrin-associated proteins in the cardiac myocyte. *Circ. Res.* **114**, 572–586
33. Kale, A., Rogers, N. M., and Ghimire, K. (2021) Thrombospondin-1 CD47 signalling: from mechanisms to medicine. *Int. J. Mol. Sci.* **22**, 4062
34. Slepian, M. J., Massia, S. P., Dehdashti, B., Fritz, A., and Whitesell, L. (1998) Beta3-integrins rather than beta1-integrins dominate integrin-matrix interactions involved in postinjury smooth muscle cell migration. *Circulation* **97**, 1818–1827
35. Bendeck, M. P., and Nakada, M. T. (2001) The beta3 integrin antagonist m7E3 reduces matrix metalloproteinase activity and smooth muscle cell migration. *J. Vasc. Res.* **38**, 590–599
36. Panchatcharam, M., Miriyala, S., Yang, F., Leitges, M., Chrzanowska-Wodnicka, M., Quilliam, L. A., *et al.* (2010) Enhanced proliferation and migration of vascular smooth muscle cells in response to vascular injury under hyperglycemic conditions is controlled by beta3 integrin signaling. *Int. J. Biochem. Cell Biol.* **42**, 965–974
37. Stouffer, G. A., Hu, Z., Sajid, M., Li, H., Jin, G., Nakada, M. T., *et al.* (1998) Beta3 integrins are upregulated after vascular injury and modulate thrombospondin- and thrombin-induced proliferation of cultured smooth muscle cells. *Circulation* **97**, 907–915
38. Janjanam, J., and Rao, G. N. (2016) Novel role of cortactin in G protein-coupled receptor agonist-induced nuclear export and degradation of p21Cip1. *Sci. Rep.* **6**, 28687
39. Hwang, C. Y., Lee, C., and Kwon, K. S. (2009) Extracellular signal-regulated kinase 2-dependent phosphorylation induces cytoplasmic localization and degradation of p21Cip1. *Mol. Cell Biol.* **29**, 3379–3389
40. Zhou, B. P., Liao, Y., Xia, W., Spohn, B., Lee, M. H., and Hung, M. C. (2001) Cytoplasmic localization of p21Cip1/WAF1 by Akt-induced phosphorylation in HER-2/neu-overexpressing cells. *Nat. Cell Biol.* **3**, 245–252
41. Chen, X., Barton, L. F., Chi, Y., Clurman, B. E., and Roberts, J. M. (2007) Ubiquitin-independent degradation of cell-cycle inhibitors by the REGgamma proteasome. *Mol. Cell* **26**, 843–852
42. Bennett, M. R. (1999) Apoptosis of vascular smooth muscle cells in vascular remodelling and atherosclerotic plaque rupture. *Cardiovasc. Res.* **41**, 361–368
43. Rossignol, P., Bouton, M. C., Jandrot-Perrus, M., Bryckaert, M., Jacob, M. P., Bezeaud, A., *et al.* (2004) A paradoxical pro-apoptotic effect of thrombin on smooth muscle cells. *Exp. Cell Res.* **299**, 279–285
44. Regan, C. P., Adam, P. J., Madsen, C. S., and Owens, G. K. (2000) Molecular mechanisms of decreased smooth muscle differentiation

marker expression after vascular injury. *J. Clin. Invest.* **106**, 1139–1147
45. Kocher, O., Gabbiani, F., Gabbiani, G., Reidy, M. A., Cokay, M. S., Peters, H., *et al.* (1991) Phenotypic features of smooth muscle cells during the evolution of experimental carotid artery intimal thickening. Biochemical and morphologic studies. *Lab. Invest.* **65**, 459–470
46. Aikawa, M., Rabkin, E., Voglic, S. J., Shing, H., Nagai, R., Schoen, F. J., *et al.* (1998) Lipid lowering promotes accumulation of mature smooth muscle cells expressing smooth muscle myosin heavy chain isoforms in rabbit atheroma. *Circ. Res.* **83**, 1015–1026
47. Weissberg, P. L., Cary, N. R., and Shanahan, C. M. (1995) Gene expression and vascular smooth muscle cell phenotype. *Blood Press. Suppl.* **2**, 68–73
48. Austin, K. M., Nguyen, N., Javid, G., Covic, L., and Kuliopulos, A. (2013) Noncanonical matrix metalloprotease-1-protease-activated receptor-1 signaling triggers vascular smooth muscle cell dedifferentiation and arterial stenosis. *J. Biol. Chem.* **288**, 23105–23115
49. Singla, B., Lin, H. P., Ahn, W., Xu, J., Ma, Q., Sghayyer, M., *et al.* (2022) Loss of myeloid cell-specific SIRPα, but not CD47, attenuates inflammation and suppresses atherosclerosis. *Cardiovasc. Res.* **118**, 3097–3111
50. Bendjennat, M., Boulaire, J., Jascur, T., Brickner, H., Barbier, V., Sarasin, A., *et al.* (2003) UV irradiation triggers ubiquitin-dependent degradation of p21(WAF1) to promote DNA repair. *Cell* **114**, 599–610
51. Li, X., Amazit, L., Long, W., Lonard, D. M., Monaco, J. J., and O'Malley, B. W. (2007) Ubiquitin- and ATP-independent proteolytic turnover of p21 by the REGgamma-proteasome pathway. *Mol. Cell* **26**, 831–842
52. Perlman, H., Maillard, L., Krasinski, K., and Walsh, K. (1997) Evidence for the rapid onset of apoptosis in medial smooth muscle cells after balloon injury. *Circulation* **95**, 981–987
53. Jagadeesha, D. K., Lindley, T. E., Deleon, J., Sharma, R. V., Miller, F., and Bhalla, R. C. (2005) Tempol therapy attenuates medial smooth muscle cell apoptosis and neointima formation after balloon catheter injury in carotid artery of diabetic rats. *Am. J. Physiol. Heart Circ. Physiol.* **289**, H1047–H1053
54. Igase, M., Okura, T., Kitami, Y., and Hiwada, K. (1999) Apoptosis and Bcl-xs in the intimal thickening of balloon-injured carotid arteries. *Clin. Sci. (Lond.)* **96**, 605–612
55. Niemann-Jönsson, A., Ares, M. P., Yan, Z. Q., Bu, D. X., Fredrikson, G. N., Brånén, L., *et al.* (2001) Increased rate of apoptosis in intimal arterial smooth muscle cells through endogenous activation of TNF receptors. *Arterioscler. Thromb. Vasc. Biol.* **21**, 1909–1914
56. Kollum, M., Kaiser, S., Kinscherf, R., Metz, J., Kübler, W., and Hehrlein, C. (1997) Apoptosis after stent implantation compared with balloon angioplasty in rabbits. Role of macrophages. *Arterioscler. Thromb. Vasc. Biol.* **17**, 2383–2388
57. Deuse, T., Hua, X., Wang, D., Maegdefessel, L., Heeren, J., Scheja, L., *et al.* (2014) Dichloroacetate prevents restenosis in preclinical animal models of vessel injury. *Nature* **509**, 641–644
58. Doran, A. C., Meller, N., and McNamara, C. A. (2008) Role of smooth muscle cells in the initiation and early progression of atherosclerosis. *Arterioscler. Thromb. Vasc. Biol.* **28**, 812–819
59. Wang, Y., Dubland, J. A., Allahverdian, S., Asonye, E., Sahin, B., Jaw, J. E., *et al.* (2019) Smooth muscle cells contribute the majority of foam cells in ApoE (apolipoprotein E)-deficient mouse atherosclerosis. *Arterioscler. Thromb. Vasc. Biol.* **39**, 876–887
60. Wang, Y., Nanda, V., Direnzo, D., Ye, J., Xiao, S., Kojima, Y., *et al.* (2020) Clonally expanding smooth muscle cells promote atherosclerosis by escaping efferocytosis and activating the complement cascade. *Proc. Natl. Acad. Sci. U. S. A.* **117**, 15818–15826
61. Koç, A., Wheeler, L. J., Mathews, C. K., and Merrill, G. F. (2004) Hydroxyurea arrests DNA replication by a mechanism that preserves basal dNTP pools. *J. Biol. Chem.* **279**, 223–230
62. Bendeck, M. P., Zempo, N., Clowes, A. W., Galardy, R. E., and Reidy, M. A. (1994) Smooth muscle cell migration and matrix metalloproteinase expression after arterial injury in the rat. *Circ. Res.* **75**, 539–545